2018-11-10

Modeling surface tension of a two-dimensional droplet using smoothed particle hydrodynamics

Ehigiamusoe, NN

10.1002/fld.4663
International Journal for Numerical Methods in Fluids
Wiley

Modelling surface tension of two-dimensional droplet using Smoothed Particle Hydrodynamics

Nowoghomwenma Noel Ehigiamusoe Samat Maxutov
Yeaw Chu Lee
School of Engineering and Physical Sciences, Heriot-Watt University,
Edinburgh, United Kingdom EH14 4AS

September 3, 2018

Abstract

Surface tension plays a significant role at the dynamic interface of free-surface flows especially at the micro-scale in capillary dominated flows. A model for accurately predicting the formation of two-dimensional viscous droplets in vacuum or gas of negligible density and viscosity resulting from axisymmetric oscillation due to surface tension is solved using Smoothed Particle Hydrodynamics (SPH) comprised of the Navier-Stokes system and appropriate interfacial conditions for the free surface boundaries. The evolution of the droplet and its free surface interface is tracked over time to investigate the effects of surface tension forces implemented using a modified Continuous Surface Force (CSF) method and is compared to those performed using Inter-particle Interaction Force (IIF). The dynamic viscous fluid and surface tension interactions are investigated via a controlled curvature model and test cases of non-steady oscillating droplets; attention is focused here on droplet oscillation that are released from an initial static deformation. Accuracy of the results are attested by demonstrating that (i) the curvature of the droplet is controlled, (ii) uniform distribution of fluid particles, (iii) clean asymmetric forces acting on the free surface, and (iv) non-steady oscillating droplets compare well with analytical and published experiment findings. The advantage of the proposed CSF method only requires the use of physical properties of the fluid whereas the IIF method is restricted by the requirement of tuning parameters.

1 Introduction

Surface tension plays a vital role in interfacial flows that is especially important at the micro-scale. It is observed ubiquitously in many capillary dominated physical processes such as in sprays, coating and printing, and occurs naturally in biological systems, for example, in water beading on leaf surfaces and tearing in eyes. The dynamics of the shape deformation of droplets are especially important in micro- and nano-fluidic applications where the surface area to volume ratios are high [1, 2].

Early theoretical work and analysis of liquid droplet oscillations has been limited to droplets that are inviscid or of negligible density and viscosity. Brown and coworkers [3, 4] analysed small- to moderate-amplitude inviscid droplet oscillations using perturbation periodic expansions that

extends Rayleigh's theory [5] on infinitesimal-amplitude oscillating spheroidal droplets. Large-amplitude droplet oscillations were studied by Lundgren and Mansour [6] for high Reynolds numbers using boundary-integral method and was followed by Patzek *et al.* [7] for low-frequency oscillations using finite-element method. Similarly, numerical models were employed by Foote [8] and Alonso [9], who investigated nonlinear large-amplitude oscillations of viscous droplets in inactive environments using the Marker-And-Cell (MAC) approach, and subsequently by Basaran [10] with the use of Galerkin finite-element method. The latter work was extended by Wilkes *et al.* [11] and among others [12, 13] that investigated the dynamics of surface tension effects on droplet formation during bifurcation, micro-threading, breakup and overturn. Other solutions for droplet formation systems, such as those by Richard *et al.* [14, 15, 16], employed the use of Volume-Of-Fluid (VOF) tracking of interfaces allow handling of highly complex, transient flow evolutions involving droplet breakups, but however lacked the ability to accurately resolve minuscule details at the interfaces due to mesh smearing numerical limitations.

The present work explores the use of Smoothed Particle Hydrodynamics (SPH), a fully Lagrangian approach, to reliably capture and model the complex dynamic behaviour of surface tension dominated droplet flows. This involves dynamic tracking of the interface caused by the unbalanced cohesion forces of fluid on the free surface, shown in Figure 1. In SPH, the fluid is represented by a system of particles that carries fluid information as it moves, making it naturally suitable for problems with complex geometries and those that undergo large deformations.

The SPH methodology, originally developed independently by Gingold and Monaghan [17] and Lucy [18] to explore astrophysical phenomena at the hydrodynamic scale, have found numerous applications in modelling fluid flow problems including moving interfaces [19]. In general, the treatment of surface tension in SPH can be broken down into 2 major groupings. The first is a macroscopic model, also referred to as the Continuum Surface Force (CSF) approach introduced in Brackbill *et al.* [20] and later popularised by Muller *et al.* [21] uses a single-phase method to track the free surface interface where a surface tension force is applied. Here, a colour field is calculated and normalised to ascertain the position of the interface and its colour gradient is used to compute the surface normal. The resulting surface tension force then acts perpendicular to the interface to minimise curvature of the free surface. While the CSF method is fast with implementations in computer graphics [22], resolving physically realistic surface tension forces offsets the performance of the methodology.

The second approach takes a microscopic view which considers cohesion forces between particles to imitate attractive forces between molecules, known as the Inter-particle Interaction Force (IIF). In Nugent and Posch [23], a cohesive pressure force was calculated using van der Waals equation of state. However, computing the latter requires the use of tuning variables, which is resolution dependent, to control the stability of the fluid particles interactions. Alternatively, Tartakovsky and Meakin [24] introduced an approach to model the cohesion force as a combined force of short-range repulsive and long-range attractive forces for droplets. This is developed further by Akinci *et al.* [25] who proposed a combine surface tension model comprising of the cohesion and surface area minimisation terms to model fluid-gas particles while an adhesion model is introduced for fluid-solid particle interactions.

In the present work, a modified single-phase CSF approach is proposed and developed to accurately model surface tension dominated flow of droplets. The proposed methodology introduces the use of a modified curvature model, where the formulation will be verified against known results numerically and those in literature. Both CSF and IIF approaches are employed to investigate the case of an oscillating water droplet with real fluid properties; the former aims to simplify and

eliminate the use of tuning parameters that may result in unphysical and unrealistic interactions.

2 Mathematical Formulation

The Navier-Stokes equations for conservation of mass and momentum in the Lagrangian form for SPH are written as follows:

$$\frac{D\rho}{Dt} = -\rho\nabla \cdot \mathbf{v}, \tag{1}$$

$$\frac{D\mathbf{v}}{Dt} = -\frac{1}{\rho}\nabla p + \frac{1}{\rho}\nabla \cdot \tau + \frac{\mathbf{F}}{\rho}, \tag{2}$$

where $\frac{D\rho}{Dt}$ is the total or material derivative, ∇ is the gradient, p is the pressure, $\mathbf{v}$ is the particle velocity, t is the time, ρ is the density (water), τ is the viscous stress tensor and $\mathbf{F}$ is the body force per unit volume that typically includes contributions such as gravity, surface tension and boundary forces.

Here, the fluid is solved using the weakly compressible [26] form which allow the pressure to be uniquely determined from the density field via an Equation of State (EOS). Solving the weakly compresible form considerably reduces the computational resources required to compute the pressure field without the need to resolve the pressure Poisson's equation for incompressible SPH [27]. Following Monaghan [26], Equations (1) and (2) are closed using Tait's EOS, given by:

$$p = B\left[\left(\frac{\rho}{\rho_0}\right)^{\gamma} - 1\right], \tag{3}$$

where $\gamma = 7$ for free-surface flows, ρ_0 is the reference density and B is the reference pressure constant:

$$B = \frac{\rho_0 c_s^2}{\gamma}, \tag{4}$$

with c_s the reference speed of sound, usually between 10 to 100 times the maximum velocity of the system in consideration, is chosen such that density variations are limited to less than 1% of the reference density [26].

3 Numerical formulation

3.1 SPH Discretization

SPH discretisation of the Navier-Stokes equations are derived from the Dirac-delta, δ, assumption that an arbitrary function:

$$f(\mathbf{r}) = \int_{\Omega} f(\mathbf{r}')\delta(\mathbf{r} - \mathbf{r}')dV, \tag{5}$$

is continuous in a domain Ω and $\mathbf{r}$ is the position vector. A smooth approximation $<f(\mathbf{r})>$ of $f(\mathbf{r})$ is obtained by replacing δ with a kernel function, W, such that:

$$< f(\mathbf{r}) >= \int_{\Omega} f(\mathbf{r}')W(|\mathbf{r} - \mathbf{r}'|, h)dV, \tag{6}$$

where h is the smoothing length of a chosen kernel.

The angular brackets <> from this point onwards is dropped for simplicity and readability. The SPH discretisation of the integral interpolant in Equation (6) is then written as:

$$f(\mathbf{r}) = \sum_{j=1}^{N} f(\mathbf{r_j}) W(|\mathbf{r} - \mathbf{r_j}|, h) dV_j, \tag{7}$$

where N corresponds to the number of the discretised particles within the domain. The finite volume, dV_j, can be replaced by the ratio of mass, m_j, to density, ρ_j, of a fluid transported by particle j. Hence, the generalised SPH approximation for $f(\mathbf{r})$ and its gradient are as follows:

$$f(\mathbf{r}) = \sum_{j=1}^{N} f(\mathbf{r_j}) \frac{m_j}{\rho_j} W(|\mathbf{r} - \mathbf{r_j}|, h), \tag{8}$$

and

$$\nabla f(\mathbf{r}) = \sum_{j=1}^{N} f(\mathbf{r_j}) \frac{m_j}{\rho_j} \nabla W(|\mathbf{r} - \mathbf{r_j}|, h). \tag{9}$$

As in finite-difference methods, the gradients in Equation (9) can be written in several ways in SPH formalism [28]. Among them are symmetric and anti-symmetric ones and interested readers are referred to Liu and Liu [29] and Violeau [28]. In the same way, several SPH forms for the divergence field can be established.

The kernel function, W, must satisfy the following conditions:

Symmetric condition:

$$W(\mathbf{r}, h) = W(-\mathbf{r}, h). \tag{10}$$

Limit condition:

$$\lim_{h \to 0} W(\mathbf{r}, h) = \delta(\mathbf{r}). \tag{11}$$

Unity condition:

$$\int_{\Omega} W(\mathbf{r}, h) d\mathbf{r} = 1. \tag{12}$$

In this study, the Wendland kernel:

$$W(q, h) = \alpha_d \begin{cases} (2 - 2q/3)^4 (1 + 4q/3) & 0 < q \leq 3 \\ 0 & q > 3, \end{cases} \tag{13}$$

where $q = |\mathbf{r}|/h$ and $\alpha_d = 7/(144\pi h^2)$ in two-dimensional space, is used mainly because is able to replicate the dissipation mechanisms more accurately. This characteristic is shown for both low and high Reynolds numbers where it prevents clustering effects from noisy vorticity fields [30].

3.2 Continuity equation

The continuity Equation (1) discretised using the SPH formulation is re-written as:

$$\frac{D\rho_i}{Dt} \approx \sum_{j}^{N} m_j \mathbf{v}_{ij} \cdot \nabla_i W_{ij}, \tag{14}$$

where i represent the particle of interest, j the neighbour particle within the support domain, ∇_i is the gradient of the kernel function with respect to particle i, $\mathbf{v}_{ij} = \mathbf{v}_i - \mathbf{v}_j$ is the relative velocity and W_{ij} is kernel function of particle i taken with respect to particle j.

Each initial particle is initialised using a reference density, ρ_0, and the rate of density change, $D\rho/Dt$, is caused by relative movement between the particles.

3.3 Momentum equation

The Navier-Stokes momentum equation is discretised in SPH with the pressure and viscosity terms using the standard forms following those in Gingold and Monaghan [31], which conserves linear and angular momentum, given by:

$$\frac{D\mathbf{v}_i}{Dt} = -\sum_{j=1}^{N} m_j \left(\frac{p_j}{\rho_j^2} + \frac{p_i}{\rho_i^2}\right) \cdot \nabla_i W_{ij} + \sum_{j=1}^{N} m_j \left(\frac{\mu_i + \mu_j}{\rho_i \rho_j}\right) \mathbf{v}_{ij} \left(\frac{1}{r_{ij}} \frac{dW_{ij}}{dr_{ij}}\right) + \mathbf{F}_i, \tag{15}$$

where μ is the fluid viscosity and $r_{ij} = |\mathbf{r_{ij}}|$ and $\mathbf{r_{ij}} = \mathbf{r_i} - \mathbf{r_j}$.

3.4 Time integration

The Verlet algorithm [32], is used for time integration. The updated density, velocity and position for each particle are calculated from the following:

$$\rho_i^{n+1} = \rho_i^{n-1} + 2\Delta t \left(\frac{D\rho_i}{Dt}\right)^n, \tag{16}$$

$$\mathbf{v}_i^{n+1} = \mathbf{v}_i^{n-1} + 2\Delta t \left(\frac{D\mathbf{v}_i}{Dt}\right)^n, \tag{17}$$

$$\mathbf{r}_i^{n+1} = \mathbf{r}_i^n + \mathbf{v}_i^n \Delta t + \frac{\Delta t^2}{2} \left(\frac{D\mathbf{v}_i}{Dt}\right)^n. \tag{18}$$

It should be noted that the time integration in Equations (16)-(18) are decoupled and an additional Euler step is required:

$$\rho_i^{n+1} = \rho_i^n + \Delta t \left(\frac{D\rho_i}{Dt}\right)^n, \tag{19}$$

$$\mathbf{v}_i^{n+1} = \mathbf{v}_i^n + \Delta t \left(\frac{D\mathbf{v}_i}{Dt}\right)^n, \tag{20}$$

at appropriate M intervals; the usual suggested value for M = 50 used to prevent the solution at odd and even steps from diverging.

The size of the time step are automatically chosen using the CFL conditions [33]. In SPH, this is given by:

$$\Delta t_1 \leq \frac{h}{c_s}, \tag{21}$$

to restrict the maximum rate of interaction propagation to not exceed the physical rate. Monaghan [34] suggested 2 additional expressions for the viscous dissipation and the external forces, given as follows:

$$\Delta t_2 = \min_i \frac{h}{c_s + 0.6(\alpha c_s + \beta \max_{i,j} \mu_{ij})}, \tag{22}$$

$$\Delta t_3 = \min_i \left(\sqrt{\frac{h}{|\mathbf{f}|}} \right), \tag{23}$$

where α and β are dimensionless coefficient, $\mathbf{f}$ is a force per unit mass, to be sure that the force exerted on particles are combined correctly.

From the above requirements the time step taken is chosen to be the minimum of Equations (21)-(23) with a safety coefficient of 1/4 as suggested by Monaghan [34]:

$$\Delta t = \frac{1}{4} \min(\Delta t_1, \Delta t_2, \Delta t_3). \tag{24}$$

3.5 Surface tension

The present work proposed a modified single phase CSF approach to the original two phase method of Brackbill *et al.* [20]. Here, the surface tension force per unit mass will be applied only to the particles on the free surface via:

$$\mathbf{f_s} = \frac{\sigma \kappa \mathbf{n} \delta_\varepsilon}{\rho}, \tag{25}$$

where κ is the local curvature, $\mathbf{n}$ is the unit surface normal vector at the interface pointing inwards to the fluid and δ_ε is the surface delta function. δ_ε is set to $1/\Delta s$ at the interface and Δs takes the value of the initial particle separation. Equation (25) is added as an additional body force in Equation (15) to provide the surface tension force.

A colour field, c, is used to determine the interface at the free surface [20]. A smoothed colour field at particle i is calculated using:

$$c_i = \sum_j^N c \frac{m_j}{\rho_j} W_{ij}, \tag{26}$$

where in the original CSF method, the above equation is employed to track the position of surface particles, but here, the following divergence of particle position proposed in Lee and Moulinec [35] is used to do the same:

$$\nabla \cdot \mathbf{r} = \sum_j \frac{m_j}{\rho_j} \mathbf{r}_{ij} \cdot \nabla_i W_{ij}. \tag{27}$$

For two-dimensional problems, $\nabla \cdot \mathbf{r}$ is approximately 2.0 for particles with a full kernel support and smaller for particles adjacent to the free surface. A threshold value of $\nabla \cdot \mathbf{r} \leq 1.5$ following Lee and Moulinec [35] is used to determine particles located at the interface. The unit surface normal in Equation (25) is calculated from the colour field gradient at the free surface with:

$$\mathbf{n_i} = \frac{\nabla c_i}{|\nabla c_i|}. \tag{28}$$

Adami *et al.* [36] proposed the approximated divergence for calculating the surface curvature using both the liquid and gas phases. However, to calculate the approximated divergence of the surface curvature using only a single liquid phase in the present study, the formulation for κ is modified by introducing a control parameter, ϵ, given by:

$$\kappa = \varepsilon \cdot d \frac{\sum_j \mathbf{n_{ij}} V_j \nabla W}{\sum_j |\mathbf{r_{ij}}| V_j \frac{\partial W}{\partial r_{ij}}}, \tag{29}$$

where d is the spatial dimension of the problem, $\mathbf{n_{ij}} = \mathbf{n_i} - \mathbf{n_j}$, V_j is the volume of the neighbour particles, and $\varepsilon = 0.5$ is found to be acceptable given that ignoring the gas phase requires that the original form in Adami *et al.* [36] to be halved.

4 Results and Discussion

4.1 Droplet Curvature

The first case explores the accuracy and validity of the proposed CFS approximated divergence curvature formulation of Equation (29) on a 2-dimensional water droplet. Following Zhang [37], a circular water droplet of radius, $R_d = 1$ mm, density, $\rho_0 = 1000$, viscosity, $\mu = 0.01$, and reference sound speed sufficient for incompressibility, $c_s = 5.0$, is considered. Here, 3 different particle resolutions were also chosen to investigate the sensitivity of the proposed CSF approach compared to the competing IIF approach [24] via initial particle spacing distribution or separation of $\Delta s = \{0.1, 005, 0025\}$ mm giving particle resolutions of $N = \{331, 1261, 4921\}$, respectively.

The circular droplet is defined uniformly to be geometrical evenly distributed using a simple algorithm to calculate their circumferential ring positions in the polar form, given by:

$$x_a = b\Delta s \cos(k\theta), \tag{30}$$

$$y_a = b\Delta s \sin(k\theta), \tag{31}$$

where a is the number of particles between $0, 1, 2, ...,$ to $(N-1)$, while b varies from $0, 1, 2, ...,$ to $(N_c - 1)$, with N_c describing the number of circular circumferential layers such that $\Delta s = R_d/(N_c - 1)$. The value for k varies between $0, 1, 2, ...,$ to $(N_p - 1)$ helps define the number of particles in each circumferential layer with $N_p = 1$ when $b = 0$ and $N_p = 6$ for subsequent layers. These particles are spread out evenly at angles given by, $\theta = 2\pi/N_p$, from one another within the same layer along the circumferential rings.

The steady-state results presented in Figure 2 shows that the approximated surface curvature formulation in CSF approach successfully captures fluid particles located at the boundary interface via Equation (27) and computing Equation (29) directs the normal uniformly and asymmetrically towards the centre of the droplet with $\kappa \approx 1$. The consistency of the CSF approach is replicated exactly with varying resolutions and the fluid particles are evenly and orderly distributed forming a perfect circular droplet. In comparison, the same case is performed using the IIF approach and the solution clearly shows large non-uniform variations in curvature values which result in uneven asymmetric force acting on the boundary interface towards the internal fluid particles, making it it difficult to recover a perfect circular shape. In addition, clumping of fluid particles at the interface due to the asymmetric build up of localised cohesion pressure forces between competing short-range repulsive and long-range attractive forces is observed and this becomes more prevalent at higher resolutions. The CSF approach shows no indications of numerical corruptions with particle resolution. Comparison with the analytical solution:

$$\kappa = \frac{1}{R}, \tag{32}$$

where R is the equilibrium radius of the droplet, showed that an error of 0.4% is observed using the CSF approach and approximately 3.0% from IIF.

Note that all subsequent results will use, R, as the equilibrium radius and, r, to represent the equatorial axis in the radial x-direction for the case of oscillating droplets.

4.2 Droplet Oscillation

The following considers the case of a 2-dimensional oscillating water droplet, 2 mm in radius, that is released from an initial oblate ellipsoidal shape at rest. An initial shape is described using the following expression:

$$\begin{pmatrix} x_i^* \\ y_i^* \end{pmatrix} = \sqrt{\frac{2}{\sin\theta}} \begin{pmatrix} x_i \sin(\theta/2) \\ y_i \cos(\theta/2) \end{pmatrix}, \tag{33}$$

where the angle, $\theta = \varepsilon\pi$, and the eccentricity, $\varepsilon = 0.55$.

The period of oscillation is given analytically by:

$$T = 2\pi\sqrt{\frac{R^3\rho}{6\sigma}}, \tag{34}$$

and using the proposed CSF approach, the period of oscillation of water is readily and naturally obtained from the computation of surface tension forces exerted on the free-surface. On the other hand, the IIF approach of Tartakovsky and Meakin [24] utilises an inter-particle surface tension force:

$$\mathbf{F}_{ij} = \begin{cases} s_{ij}\cos\left(\dfrac{1.5\pi}{3h}|\mathbf{r}_{ij}|\right)\dfrac{\mathbf{r}_{ij}}{|\mathbf{r}_{ij}|}, & |\mathbf{r}_{ij}| \le 3h \\ 0, & |\mathbf{r}_{ij}| > 3h, \end{cases} \tag{35}$$

where $\mathbf{F}_{ij}$ is the pair-wise molecular force (body force) while s_{ij} is the strength of the force between particles and its value depends on the type of fluid used. In the present case $s_{ij} = 0.012$ corresponds to water for the same droplet size.

Figure 3 shows the evolution of droplet radius with time taken along the cross-section in the x-direction. Both the IIF and CSF methods yields the same analytical period of 0.027 s for water with an approximate error of 0.5%. However, the results showed that the IIF approach damps very quickly and reaches steady state in only 4 oscillations with a cut off amplitude of 2.125 mm. This is due to the ever-present dissipating internal inter-particle forces within the droplet. On the contrary, the droplet modelled using the proposed CSF approach oscillates far longer and damps out in approximately 60 oscillations. Comparisons with experimental results in Apfel *et al.* [38] reported that a squeezed droplet of 6.6 cm^3 in micro-gravity oscillates as much as 82 times. The results obtained from the proposed CSF approach was performed in 2-dimensions and one would expect that the surface tension contribution would be smaller and thus the number of oscillations will be fewer compared to 3-dimensional ones.

Figure 4 shows the droplet oscillation snapshots taken at fixed time intervals to compare droplet evolution and particle distribution of both CSF and IIF approaches in SPH. It clearly shows the resultant distinctive particle arrangements between both methodologies. The former has an obvious particle layer at the free surface interface due to the asymmetrical internal inter-particle forces and has been similarly observed in Nugent and Posch [23]. The CSF approach shows a much cleaner and evenly distribution of particles. The use of the Wendland kernel contributed to minimising the effect of tensile instability [30] while the surface tension forces act only at the interface boundaries. Small voids can be seen for these particle resolution, especially during the initial first few oscillations, but these disappear when high particle resolution are used, see Figure 5. In addition, droplets at higher resolution tend to hold their shape better but this does not mean that they oscillate larger in amplitude and longer in time. Figure 6 shows the maximum oblate amplitude of the oscillating droplet decay from the equatorial axis at long time scales using the CFS approach. The reduction

in amplitude of the oscillating droplet maintains roughly the same rate initially and shows that as the resolution increases, the amplitude of the oscillation decays much faster and resulted in slightly smaller number of total oscillations, inline with what one would expect from a more tightly packed distribution.

The effect of using the weakly compressible assumption is supported by analysing the changes in density over the first period of oscillation where changes in density is largest. This is shown in Figure 7 that the maximum error in density variation is worst at $t = 0.015s$ giving an error value of 0.6%. Nonetheless, the overall density profile is relatively smooth and this smooth variation persist throughout the remaining oscillations. The results obtained are consistent and accurate within acceptable limits with those of the weakly compressible assumption given in Monaghan [26].

5 Conclusion

A new proposed CSF approach for capturing the surface tension effects on the evolution of free surface oscillation of droplets is implemented by incorporating an adaptive SPH interface tracking scheme. To demonstrate its effectiveness, the proposed method is compared against a rival IIF approach and with those reported in literature. From the results, the CSF method yields a period of oscillation comparable to the analytical period of 0.027 s for water. Based on the above, the CSF approach can be readily applied without the need to tune arbitrary variables compared to the requirement in the IIF approach, due to the latter having to specify the inter-particle surface tension force strength. Moreover, the CSF approach is able to predict the oscillation of droplets with good qualitative results similar to those observed experimentally and also produces more ordered particle distributions. Future work will include extending the model to investigate 3-dimensional surface tension dominated flows in oscillating droplets and their potential applications in micro-mixing processes such as those observed in coalescence of binary drops.

6 Acknowledgement

Nowoghomwenma Noel Ehigiamusoe wishes to express his profound gratitude to TETFUND of Nigeria with reference No. TETFUND/ES/AST&D/AAU/EKPOMA/VOL.4 for providing the scholarship to do this research, without which it would have been impossible to accomplished this task.

References

[1] AA Darhuber and SM Troian. Principles of mircofluidic actuation by modulation of surface stresses. *Annual Review of Fluid Mechanics*, 37:435–455, 2005.

[2] R Mukhopadhyay. Dicing into droplets. *Analytical Chemistry*, 78(5):1401–1404, 2006.

[3] JA Tsamopoulos and RA Brown. Nonlinear oscillations of inviscid drools and bubbles. *Journal of Fluid Mechanics*, 127:519–537, 1983.

[4] R Natarajan and RA Brown. Third-order resonance effects and the nonlinear stability of drop oscillations. *Journal of Fluid Mechanics*, 183:95–121, 1987.

[5] L Rayleigh. On the capillary phenomena of jets. *Proceedings of the Royal Society of London*, 29:71–97, 1879.

[6] TS Lundgren and NN Mansour. Oscillation of drops in zero gravity with weak viscous effects. *Journal of Fluid Mechanics*, 194:479–510, 1988.

[7] TW Patzek, RE Benner, OA Basaran, and LE Scriven. Nonlinear oscillations of inviscid free drops. *Journal of Computational Physics*, 97:489–515, 1991.

[8] GB Foote. A numerical method for studying simple drop behaviour: simple oscillation. *Journal of Computational Physics*, 11:507–530, 1973.

[9] CT Alonso. The dynamics of colliding and oscillating drops. *Proceedings of the International Colloquium on Drops and Bubbles*, 1:139–157, 1974.

[10] OA Basaran. Nonlinear oscillations of viscous liquid drops. *Journal of Fluid Mechanics*, 241:169–198, 1992.

[11] ED Wilkes, SD Phillips, and OA Basaran. Computational and experimental analysis of dynamics of drop formation. *Physics of Fluids*, 11(12):3577–3598, 1999.

[12] RMSM Schulkes. The evolution and bifurcation of a pendant drop. *J. of Fluids Mech.*, 278:83, 1994.

[13] DF Zhang and HA Stone. Drop formation in viscous flows at a vertical capillary tube. *Phys. of Fluids*, 9:2234, 1997.

[14] JR Richards, AN Beris, and AM Lenhoff. Steady laminar flow of liquid-liquid jets at high reynolds numbers. *Phys. of Fluids*, 5:1703, 1993.

[15] JR Richards, AM Lenhoff, and AN Beris. Dynamic breakup of liquid-liquid jets. *Phys. of Fluids*, 6:2640, 1994.

[16] JR Richards, AN Beris, and AM Lenhoff. Drop formation in liquid-liquid systems before and after jetting. *Phys. of Fluids*, 7:2617, 1995.

[17] RA Gingold and JJ Monaghan. Smoothed Particle Hydrodynamics: Theory and application to non-spherical stars. *Royal Astronomical Society, Monthly Notices*, 181:375–389, 1977.

[18] LB Lucy. A numerical approach to the testing of the fission hypothesis. *The Astronomical Journal*, 82:1013–1024, 1977.

[19] K Szewc, J Pozorski, and JP Minier. Analysis of the incompressibility constraint in the Smoothed Particle Hydrodynamics Method. *International Journal for Numerical Methods in Engineering*, 92(4):343–369, 2012.

[20] JU Brackbill, DB Kothe, and C Zemach. A continuum method for modelling surface tension. *J Comput Phys*, 100:335–354, 1992.

[21] M Muller, D Charypar, and M Gross. Particle-Based Fluids Simulation for Interactive Applications. *Eurographics/SIGGRAPH Symposium on Computer Animation*, (154–372), 2003.

[22] M Imhsen, J Orthmann, B Solenthaler, A Kolb, and M. Teschner. SPH fluids in computer graphics. *Eurographics 2014 - State of the Art Reports*, 2014.

[23] S Nugent and HA Posch. Liquid drops and surface tension with smoothed particle applied mechanics. *Phys. Rev. E*, 62(4):4968–4975, 2000.

[24] AM Tartakovsky and P Meakin. Modelling of surface tension and contact angles with smoothed particle hydrodynamics. *Phys. Rev. E*, 72:026301, 2005.

[25] N Akinci, G Akinci, and M Teschner. Versatile Surface Tension and Adhesion for Smoothed Particle Hydrodynamics Fluids. volume 32 of *ACM Transactions on Graphics TOG- Proceedings of ACM SIGGRAPH Asia*, New York, NY, USA, November, 2013. 182:1–8.

[26] JJ Monaghan. Simulating free surface flows with SPH. *J Comput Phys*, 110(2):399–406, 1994.

[27] ES Lee. Truly incompressible approach for computing incompressible flow in SPH and comparisons with the traditional weakly compressible approach. *PhD thesis, University of Manchester (UK)*, 2007.

[28] D Violeau. Fluid Mechanics and the SPH Method: Theory and Applications. *Oxford University Press, UK*, 2012.

[29] GR Liu and MB Liu. Smoothed Particle Hydrodynamics: A Mesh-free Particle Method. *Covert Garden, London*, 149, 2003.

[30] F Macia, M Antuono, and A Colagrossi. Benefits of using a Wendland kernel for free-surface flows. 6^{th} International SPHERIC workshop, Hamburg, Germany, June 8–10, 2011.

[31] RA Gingold and JJ Monaghan. Kernel estimates as a basis for general particle methods in hydrodynamics. *J Comput Phys*, 46(3):429–453, 1982.

[32] L Verlet. Computer experiments on classical fluids. I. Thermodynamical properties of Lennard-Jones molecules. *Phys. Rev*, 159(1):98–103, 1967.

[33] R Courant, K Friedrichs, and H Lewy. Uber die partiellen differenzengle-ichungen der mathematischen physik. *Mathematische Annalen*, 100:32–74, 1928.

[34] JJ Monaghan. Smoothed Particle Hydrodynamics. *Annual Review of Astronomy and Astrophysics*, 30:543–574, 1992.

[35] ES Lee, C Moulinec, R Xu, D Violeau, D Laurence, and P Stansby. Comparisons of weakly compressible and truly incompressible algorithms for the SPH mesh free particle method. *J. of Comp. Phys*, 227:8417–8436, 2008.

[36] S Adami, XY Hu, and NA Adams. A new surface-tension formulation for multi-phase SPH using a reproducing divergence approximation. *J. of Comp. Phys*, 229(13):5011–5021, 2010.

[37] M Zhang. Simulation of surface tension in 2D and 3D with smoothed particle hydrodynamics method. *J. of Comp. Phys*, 229(19):7238–7259, 2010.

[38] RE Apfel, Y Tian, J Jankovsky, T Shi, X Chen, Holt R Glynn, E Trinh, A Croonquist, KC Thornton, A Sacco, C Coleman, FW Leslie, and Matthiesen DH. Free Oscillations and Surfactant Studies of Superdeformed Drops in Microgravity. *Physical Review Letters*, 78(10), 1997.

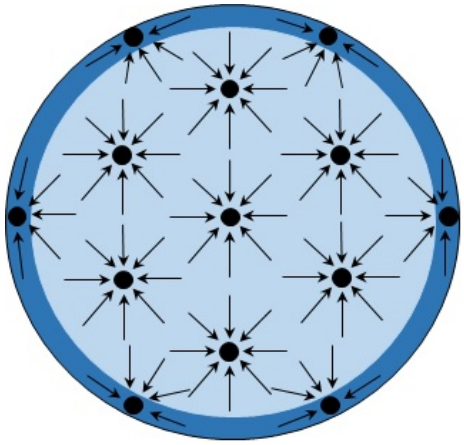

Figure 1: Unbalanced surface tension force at the interface of a fluid droplet.

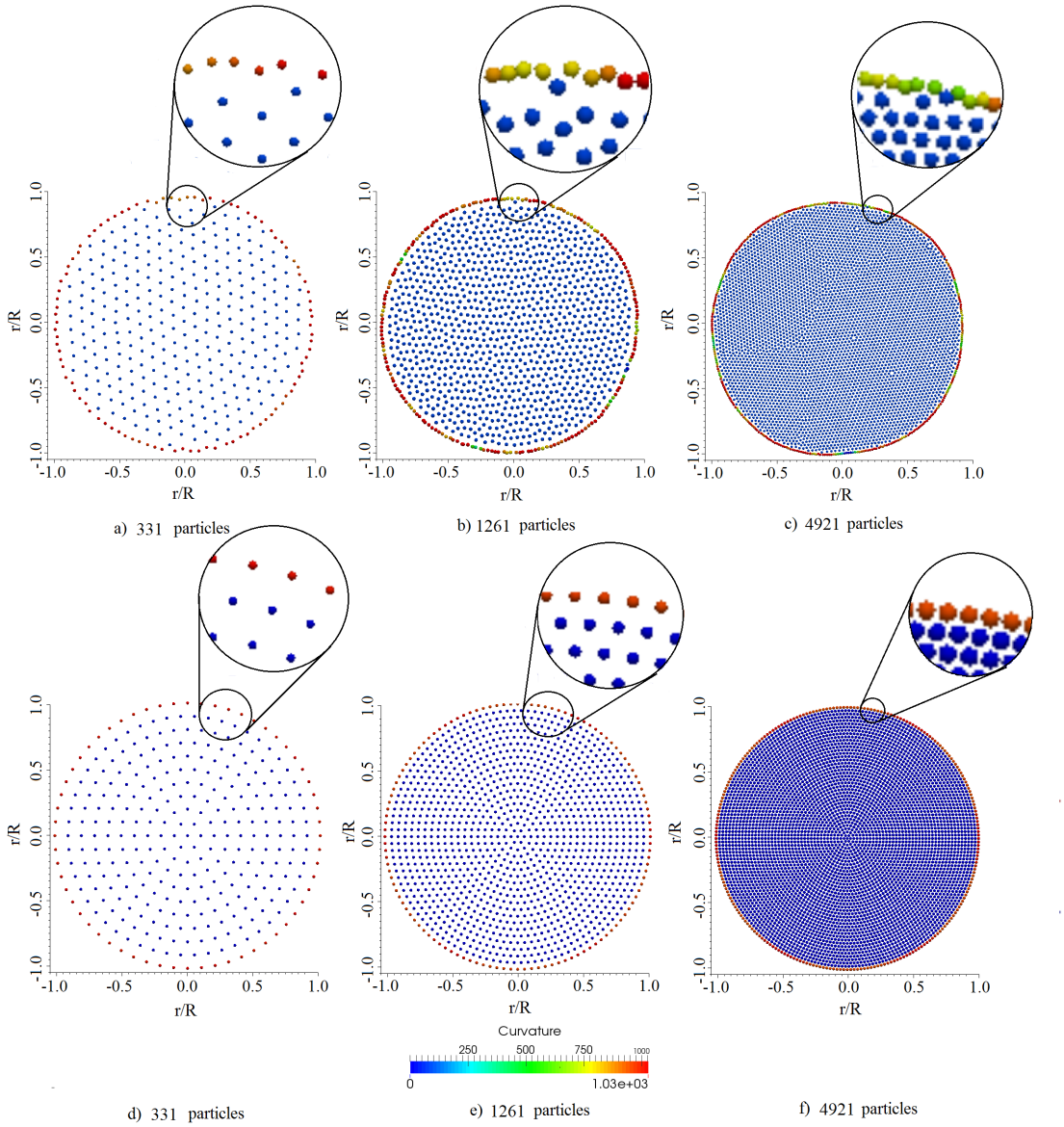

Figure 2: Steady-state droplet shape with curvature values applied at the interface at different resolutions using (i) the IIF approach (a) to (c), and (ii) the proposed CSF approach (d) to (f). Colours on the interface indicates the uniformity of the asymmetric force from the divergence of surface curvature exerted on the internal fluid particles.

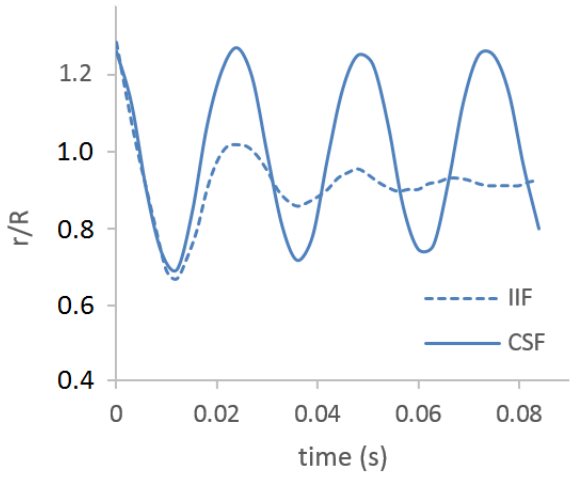

Figure 3: Time evolution of the droplet radius displacement from the equatorial axis in the radial x-direction of the oscillating droplet as it evolves between the 2-dimensional prolate and oblate modes in SPH using the IIF and proposed CSF approaches.

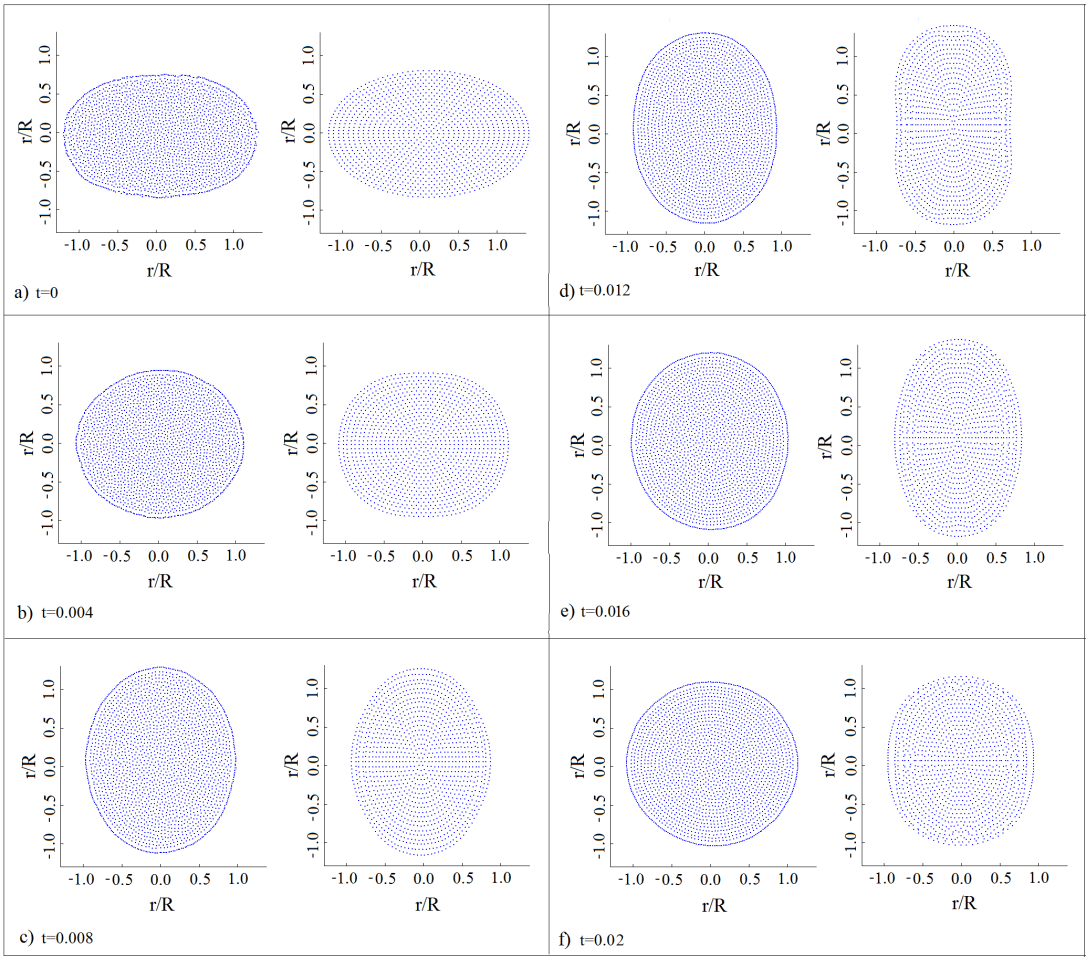

Figure 4: Evolution of the droplet oscillation at different time intervals using the IIF (left) and proposed CSF (right) approaches. The IIF approach clearly shows clumping of fluid particles at the interface due to the build up of cohesion pressure forces between competing short-range repulsive and long-range attractive forces, while the CFS approach provides better particle distribution uniformity but at times the internal layer below the interface may exhibit small void pockets.

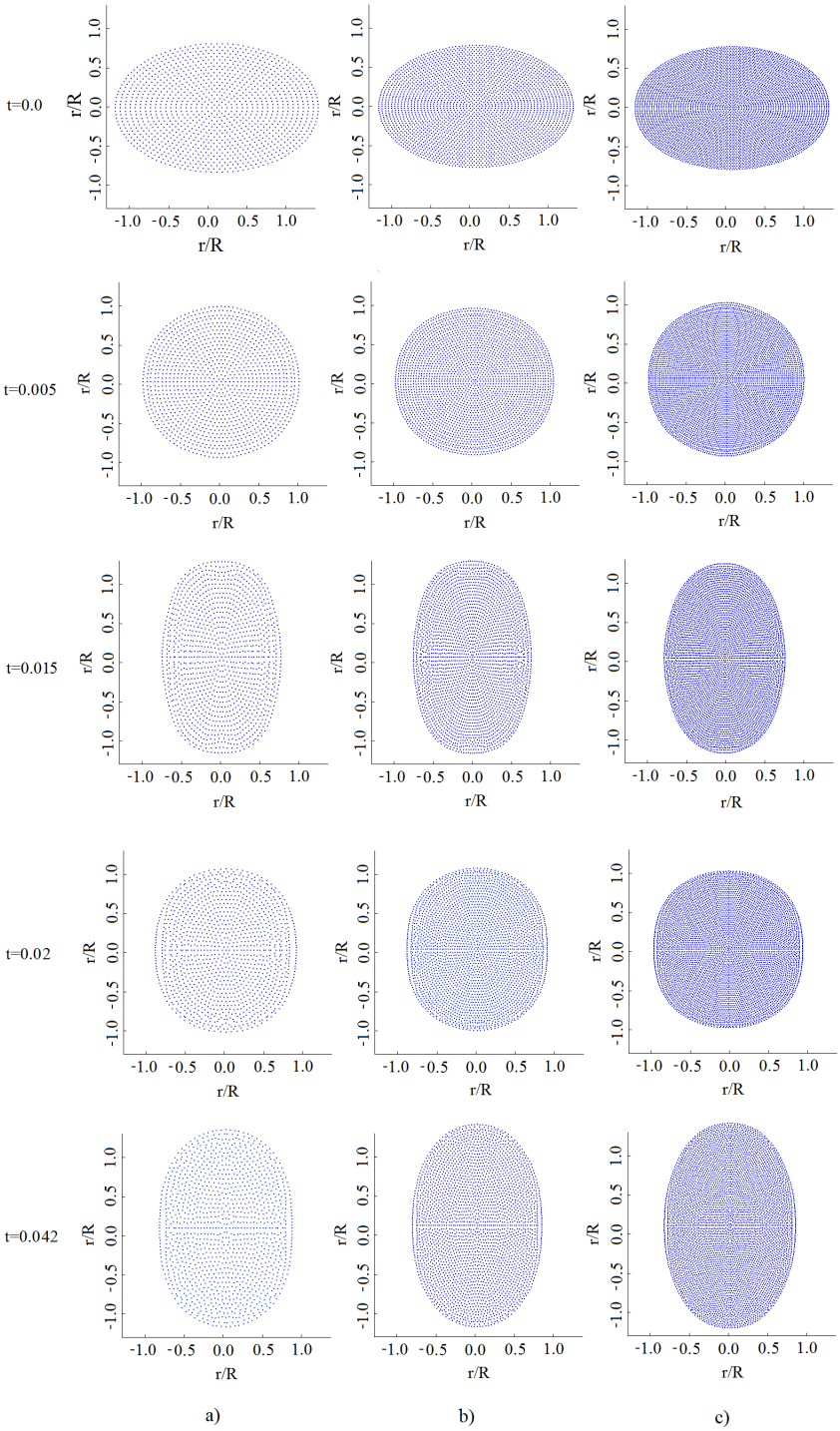

Figure 5: Droplet oscillation snapshots taken at different time intervals using the proposed CSF approach computed at different particle resolutions: (a) 1261, (b) 2791, and (c) 4921. The void pockets disappear with improved resolution and the period of oscillation stayed the same throughout the solution.

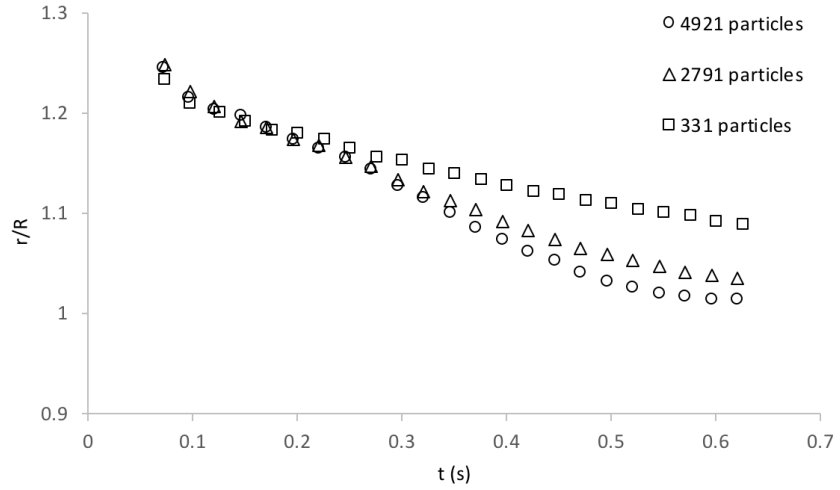

Figure 6: Maximum oblate amplitude of the oscillating droplet decay from the equatorial axis in the radial x-direction for long time scales computed using the CSF approach at different SPH particle resolutions.

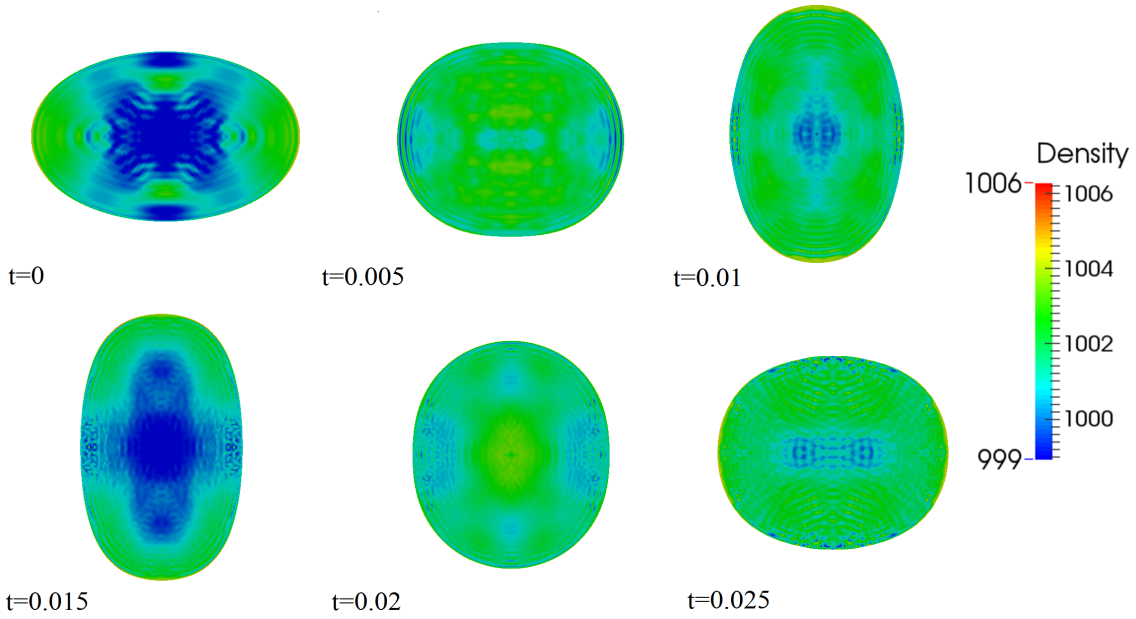

Figure 7: Density distribution of the oscillating droplet using the proposed SPH CSF approach at different time intervals during the first period of oscillation. The droplet is initially released from rest at $t = 0$ with a static shape defined in an oblate 2-dimensional mode.